Iraqi Journal of Physics, 2021
DOI: 10.30723/ijp.v19i50.629

Vol. 19, No. 50, PP. 20-30
P-ISSN: 2070-4003
E-ISSN: 2664-5548

Toxic Gas Response for Nanostructured Cobalt Oxide Thin Films

Suhad A. Hamdan[*], Iftikhar M. Ali[a], Issam M. Ibrahim[b]
Department of Physics, College of Science, University of Baghdad, Baghdad, Iraq
[a]E-mail: iftikhar.ali@sc.uobaghdad.edu.iq, [b]E-mail: Isam.ibrahim@sc.uobaghdad.edu.iq
[*]Corresponding author: suhad.a@sc.uobaghdad.edu.iq

Abstract

The gas sensing properties of undoped Co_3O_4 and doped with Y_2O_3 nanostructures were investigated. The films were synthesized using the hydrothermal method on a seeded layer. The XRD, SEM analysis and gas sensing properties were investigated for the prepared thin films. XRD analysis showed that all films were polycrystalline, of a cubic structure with crystallite size of (12.6) nm for cobalt oxide and (12.3) nm for the Co_3O_4:6% Y_2O_3. The SEM analysis of thin films indicated that all films undoped Co_3O_4 and doped possessed a nanosphere-like structure.

The sensitivity, response time and recovery time to H_2S reducing and NO_2 oxidizing gases were tested at different operating temperatures. The resistance changed with exposure to the test gas. The results revealed that the Co_3O_4:6%Y_2O_3 possessed the highest sensitivity around 90% (at room temperature) and 62.5% (at 150 ^oC) when exposed to the reducing gas H_2S and oxidizing gas NO_2, respectively with 0.8sec for both recovery and response times.

Article Info.

Key words:
Cobalt Oxide, Yttrium, gas Sensor, Sensitivity, Hydrothermal.

Article history:
Received: Sep. 30, 2020
Accepted: Jun. 04, 2021
Published: Sep. 01, 2021

1. Introduction

Among all types of gas sensors, metal oxide chemoresistive MOS gas sensor, may be the most interesting type because of its low cost, high stability, and easy integration with electronics [1]. The sensitivity and selectivity of MOS gas sensor have been improved significantly by doping the metal oxides with other catalytic metals [2].

The response of a metal oxide surface strongly depends on the composition of atmosphere; especially water (wet atmosphere) and oxygen (dry atmosphere) which defines the baseline for the sensor response and calibration. Rapid industrial growth and increase in automobiles have led to drastic intensification in the concentration of toxic and hazardous gases in the atmosphere. These gases can be classified as oxidizing (e.g.O_2, CO_2, NO_2) since they accept electrons from the metal oxide surface and reducing for they act as electron donors when interacting with metal oxide surface (e.g. CO, SO_2, NH_3, H_2S, C_2H_5OH gases) [3]. Metal oxides used in MOS gas sensors can be divided into n- type or p-type depending on their charge carrier type. N-type metal oxides are widely used as sensitive materials [4].

The gas sensor based on Cobalt oxide (Co_3O_4) is a p-type semiconductor with a spinal structure. The Co^{2+} ions occupy one-eighth of the tetrahedral sites and Co^{3+}ions occupy half of the octahedral sites [5]. Cobalt oxide has direct optical band gaps at 1.48 and 2.19 eV [6]. Hydrothermal synthesis can be defined as a technique that depends on the solubility of minerals in hot environment under high pressure to obtain interested nanostructures where the crystal growth is achieved in a tool consisting of a steel pressure vessel called an autoclave [7]. The gas sensing property of the sensor was improved significantly which may be due to the catalyst effect in the addition of yttrium nanoparticles in the structure of metal oxide.

The structural and sensing properties for H_2S reduction and NO_2 oxidizing gases were examined. The interaction of gases with films will be discussed. The temperature requirements of the sensor signal and the values of recovery time and response time was calculated.

2. Experimental work

Undoped Co_3O_4 and doped Co_3O_4:Y_2O_3 thin films were prepared using the hydrothermal method onto a seeded layer. Firstly, to prepare the seeded layer, PVA $(C_4H_6O_2)_n$ was used, which was dissolved in distilled water. The aqueous solutions of cobalt nitrate and Yttrium nitrate with 0.1M were stirred separately in a magnetic stirrer for 10 min to prepare the precursors which are the sources of cobalt and yttrium ions. Then, a cobalt precursor was added to 1.5 g of PVA at 80^{o}C for 2hours. This solution was irradiated with 2.4 GHz microwave frequency of 220W power for 10 min, then the pH of the solution was measured and its value was changed to 8or until the color of the solution changed. The resultant solution was spin coated onto silicon and glass substrates at 1500 rpm for 1 min, this step was repeated several times to obtain the desired thickness for the seed layer.

The above steps are for the preparation of pure seed layer solution. To prepare a seed layer solution with yttrium, the same steps were carried out but two different salts, cobalt nitrate, and yttrium nitrate were mixed in a magnetic stirrer for 1 h at 70^{o}C before adding a PVA solution. Finally, these seed layers were dried at 120 ^{o}C for a few minutes to achieve suitable adhesion of the seeded particles onto the surface of the substrate. The chief purpose of using seed layer is to supply nucleation locations by weakening the thermodynamic barrier between heterogeneous materials. An additional advantage that has been detected is that when seed layer was used, the grown nanostructures were found to be well aligned, greatly dense and uniform. These seeded layers were thermally annealed at 210^{o}C for 1h to remove the PVA, then annealed at 380 ^{o}C for 2h to improve crystallinity and remove the hydroxide phase. The next step is the growth process.

To prepare a growth solution, 0.1M cobalt nitrite (as a source of cobalt ions) and 0.1M Hexamine $C_6H_{12}N_4$ (as an oxidized agent) were dissolved separately in distilled water and stirred for 10 min. Then, these two solutions were mixed together and stirred for 10 min. For Co_3O_4:Y_2O_3 preparation, the same procedure was conducted, but before adding hexamine, yttrium nitrate (as a source of yttrium ions) was added to cobalt nitrate in an appropriate amount and stirred together at 70^{o}C for 1h to permit these two elements to disperse well, and then after 1h hexamine was added. The mixture was transferred into a Teflon-lined stainless-steel autoclave where the substrates with seeded layers were vertically aligned inside the Teflon container by help of a Teflon sample holder facing downward in the autoclave.
The autoclave was sealed with haste and kept at 100^{o}C for 4h in a digital temperature-controlled oven. Afterwards, the autoclave was cooled to room temperature naturally. The substrates were washed with distilled water to eliminate any residual solid particles from the surface or unreacted atoms, and then the samples were dried in oven at 100^{o}C for 30 min. The annealing process was done inside a furnace at 500^{o}C for 1h to convert the hydroxide phase $Co(OH)_2$ into Co_3O_4. Therefore, the films are ready to be characterized.

The autoclave features a shell that is made of stainless steel (SS304), with temperature ranges between (100-300) ^{o}C, a capacity of 100ml, and a pressure of <= 3Mpa (Toption Instrument Co. Limited, China). A pure aluminum e finger-shaped metal contacts act as electrodes with a thickness of 250nm were deposited on top of

the Co_3O_4:Y_2O_3 thin films, using an E306A Edwards thermal evaporation system under high vacuum of 5-10 mbar by rotary.

The structural properties were determined by X-ray diffraction (XRD- 6000 Labx, supplied by Shimadzu, X-ray source Cu). Film morphology was analyzed with a MIRA3 model – TE-SCAN, Field Emission Scanning Electron Microscope (FESEM). The measurements of the Hall effect were performed by Van der Pauw (Ecopia HMS3000) Hall measurement systems using (0.55 Tesla) magnetic field.

3. Results and discussion

3.1. Structural properties (XRD)

X-ray diffraction patterns of synthesized undoped Co_3O_4 and doped with Yttria grown onto silicon substrates are shown in Fig.1. It can be noticed that the patterns exhibit diffraction peaks around (2θ~ 31.5º, 37º, 38.8º, 44.9º, 56º, 59.6º and 65.3º) referred to (202), (311), (222), (400), (422), (333) and (404) favorite directions, respectively for Co_3O_4. This is in agreement with JCPDS card number 96-900-5888 which proves the cubic structure for hydrothermally prepared cobalt oxide and illustrates the presence of Co_3O_4 phase. In addition to these peaks, it can be noticed that the patterns exhibit diffraction peaks around (2θ~ 33.8º, 48.7ºand 57.8º) referred to (400), (440) and (622) favorite directions, respectively for yttria, which is in agreement with JCPDS card number 96-100-9018. The data of peaks positions and miller indices for the diffracting planes and FWHM are shown in Table 1. It is noticed that, for doping 2 and 4 wt. % Y_2O_3, there were no new peaks i.e., no new compound was formed. This may be due to the low proportion of Y_2O_3. At doping ratio of 6 wt. % Y_2O_3, new characteristic peaks belonging to Y_2O_3 phase appeared and the structure of the prepared films is still polycrystalline with cubic structure according to JCPDS (standard card NO.96-900-5888). As for 6 %Y_2O_3, the (400) and (440) planes appeared located at (2θ and comparis=34.5º, 49.7º), respectively in agreement with Cosentino and Muccillo [8]. The (311) plane as the preferential orientation agrees with the results of Cheng et al. [9] and Lakehal et al. [10]. Crystallite size is estimated by Scherrer's formula [11]:

$$D = \frac{K\lambda}{\beta cos\theta} \qquad (\mathbf{1})$$

In this equation, shape factor (K)=0.9, λ represents the wavelength of the X-ray radiation, β is the full width at half maximum of the diffraction peak (in radians) and θ is Bragg diffraction angle of the diffraction peak. The maximum value of average crystallite size D_{ave} was 12.6 nm for undoped cobalt oxide and the minimum value was 12.3 nm for doped cobalt oxide with 6% Y_2O_3.

The average crystallite size decreased with adding yttria. The crystallite size deceased with increasing Y_2O_3 doping ratio which consequently led to increase in FWHM. Decreasing in the crystallite size after doping is evidence on the enhancement of the nanocrystal, thus one can conclude that modulation of Y_2O_3 in the precursor solution reduces the crystallite size which proves that the deposited atoms of these films are going towards nanostructure. The lattice constant a_{exp}. Of the unit cell was calculated from predominated orientation (311) using the following equation [11]:

$$d = \frac{a}{(h^2 + k^2 + l^2)^{\frac{1}{2}}} \qquad (\mathbf{2})$$

where hkl are Miller indices.

Table 1 displays structural parameters calculated from XRD spectra for cobalt oxide and cobalt yttrium oxide. The calculated lattice constant of the cobalt oxide nanostructure and d_{hkl} (the interplaner spacing) were calculated using Bragg's law [11]:

$$2d_{hkl}sin\theta = n\lambda \qquad (\mathbf{3})$$

where d is the spacing between the planes, θ is the angle that the X-ray beam makes with respect to the plane, λ is the wavelength of the X rays, and n = 1,2,3, . . . is an integer that usually has the value n= 1. The results are tabulated in Table 2. The standard value of lattice constant for Co_3O_4 is 8.083 Å close to the one given by JCPDS (standard card No.96-900-588). The results indicate the decrease in lattice constant of Co_3O_4 with the increase of doping, with maximum value for the undoped Co_3O_4, may be the doping makes vary lightly in lattice constant.

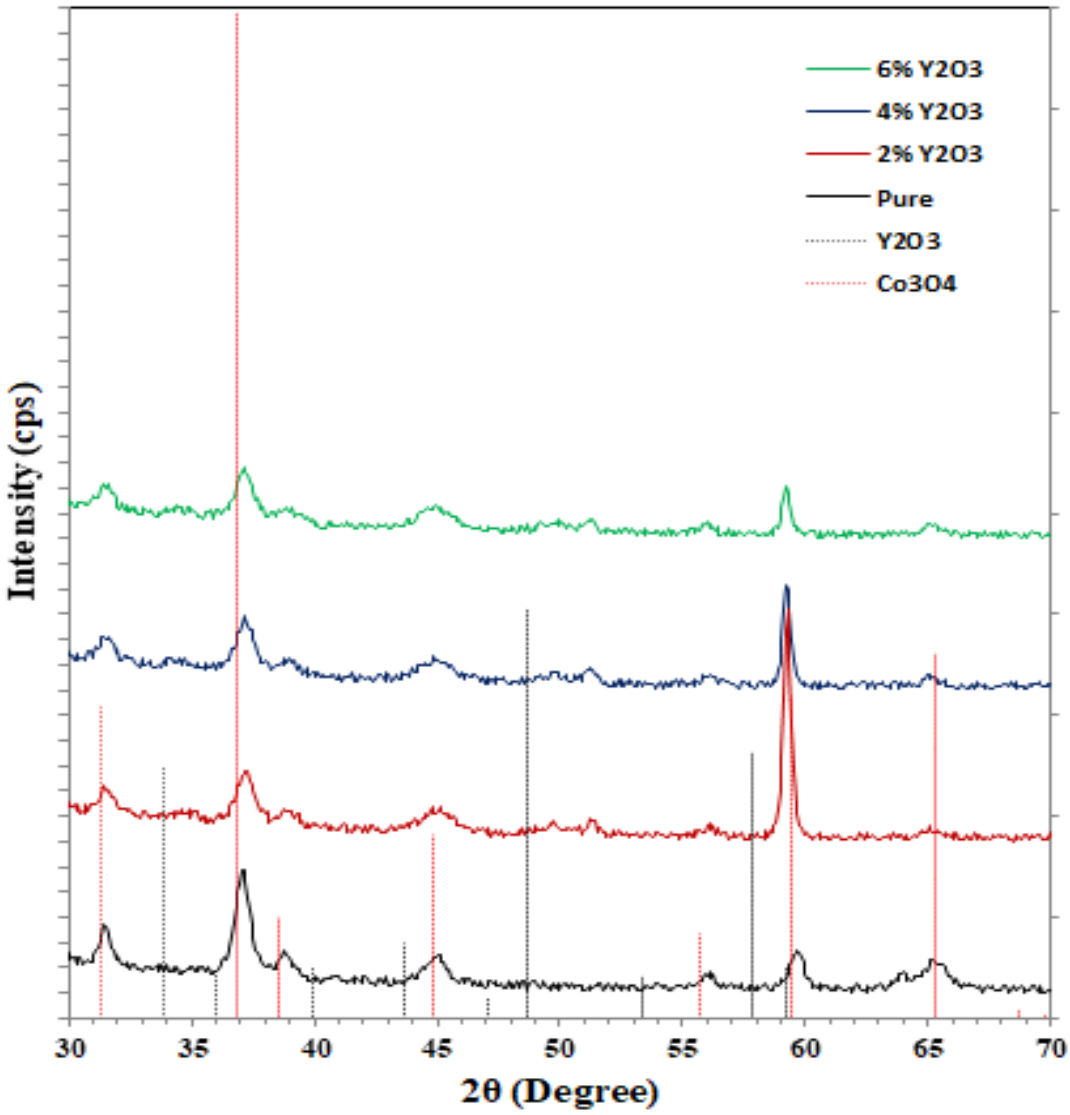

Figure 1: XRD patterns for undoped Co_3O_4 thin film and doped with (2, 4, and 6) %wt. of yttria thin films deposited on n-Si substrate by hydrothermal method.

Table 1: Structrure Parameters for for undoped Co_3O_4 and doped with (2, 4, and 6) % wt. of yttria thin films deposited on n-Si substrate by hydrothermal method.

Y%	2θ (Deg.)	FWHM (Deg.)	d_{hkl} Exp.(Å)	D (nm)	D_{ave} (nm)	hkl	d_{hkl} Std.(Å)	Phase	Card No.
0	31.504	0.477	2.837	17.3	12.6	(202)	2.858	Co_3O_4	96-900-5888
	37.079	0.716	2.422	11.7		(311)	2.437	Co_3O_4	96-900-5888
	38.849	0.637	2.316	13.2		(222)	2.334	Co_3O_4	96-900-5888
	44.955	1.035	2.014	8.3		(400)	2.021	Co_3O_4	96-900-5888
	56.017	0.637	1.640	14.1		(422)	1.649	Co_3O_4	96-900-5888
	59.646	0.637	1.548	14.4		(333)	1.555	Co_3O_4	96-900-5888
	65.309	1.035	1.427	9.1		(404)	1.428	Co_3O_4	96-900-5888
2	31.521	0.797	2.835	10.4	12.6	(202)	2.858	Co_3O_4	96-900-5888
	37.193	0.797	2.415	10.5		(311)	2.437	Co_3O_4	96-900-5888
	38.966	0.886	2.309	9.5		(222)	2.334	Co_3O_4	96-900-5888
	44.992	1.506	2.013	5.7		(400)	2.021	Co_3O_4	96-900-5888
	56.070	0.620	1.638	14.5		(422)	1.649	Co_3O_4	96-900-5888
	59.261	0.354	1.558	25.8		(333)	1.555	Co_3O_4	96-900-5888
	65.130	0.797	1.431	11.8		(404)	1.428	Co_3O_4	96-900-5888
4	31.500	0.808	2.837	10.2	12.4	(202)	2.858	Co_3O_4	96-900-5888
	37.172	0.808	2.416	10.4		(311)	2.437	Co_3O_4	96-900-5888
	38.944	0.898	2.310	9.4		(222)	2.334	Co_3O_4	96-900-5888
	44.971	1.526	2.014	5.6		(400)	2.021	Co_3O_4	96-900-5888
	56.049	0.628	1.639	14.3		(422)	1.649	Co_3O_4	96-900-5888
	59.240	0.359	1.558	25.5		(333)	1.555	Co_3O_4	96-900-5888
	65.090	0.808	1.431	11.7		(404)	1.428	Co_3O_4	96-900-5888
6	31.478	0.818	2.839	10.1	12.3	(202)	2.858	Co_3O_4	96-900-5888
	34.580	1.182	2.591	7.0		(400)	2.643	Y_2O_3	96-100-9018
	37.150	0.818	2.418	10.2		(311)	2.437	Co_3O_4	96-900-5888
	38.923	0.909	2.312	9.3		(222)	2.334	Co_3O_4	96-900-5888
	44.949	1.546	2.015	5.6		(400)	2.021	Co_3O_4	96-900-5888
	49.735	1.273	1.831	6.9		(440)	1.868	Y_2O_3	96-100-9018
	56.028	0.636	1.640	14.1		(422)	1.649	Co_3O_4	96-900-5888
	59.218	0.363	1.559	25.1		(333)	1.555	Co_3O_4	96-900-5888
	65.120	0.818	1.431	11.5		(404)	1.428	Co_3O_4	96-900-5888

Table 2: Lattice constant for undoped Co_3O_4 and doped with (2, 4, and 6) %wt. of yttria.

$\%Y_2O_3$	$a_{exp.}$ (A°)	$a_{std.}$ (A°)
0	8.034	8.084
2	8.010	
4	8.015	
6	8.019	

3.2. Field Emission Scanning Electron Microscope (FESEM)

FESEM measurements were used to analyze the grain size and surface morphology of the seeded layers which were prepared using spin coating technique and that of the grown layer prepared by hydrothermal method for undoped Co_3O_4 and

doped with Y_3O_2 thin films. Fig.2 illustrates the images for seed layer and growth film of undopedCo_3O_4 nanoparticle. These images reveal the distribution of sphere shaped particles on a smooth surface which is in agreement with Mohamed & Samson [12], Yarestani et al. [13], and Farhadi et al. [14].

The doping with Y_2O_3 influences the surface morphology of the sample. SEM images of seed layer and doped $Co_3O_4$with 2wt. % Y_2O_3 nanoparticles are shown in Fig.3. It is obvious that the prepared nanoparticles are in a cluster form. Grain boundaries are very clear especially for Co_3O_4 doped with 4wt. %Y_2O_3 and 6wt. % Y_2O_3 as shown in Figs. 4 and 5, respectively. The cobalt oxide film surface is well covered without any pinholes and cracks. Such surface morphology may offer increased surface area, feasible for gas sensing applications and this in agreement with Shinde et al. [15] and Gujar et al. [16].

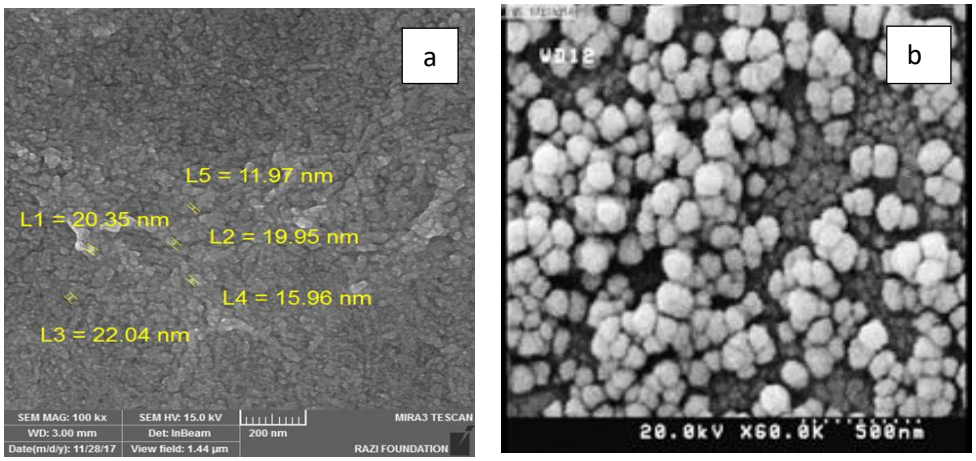

Figure 2: FESEM images of undopedCo_3O_4 thin film: (a) Seed layer, (b) Growth layer.

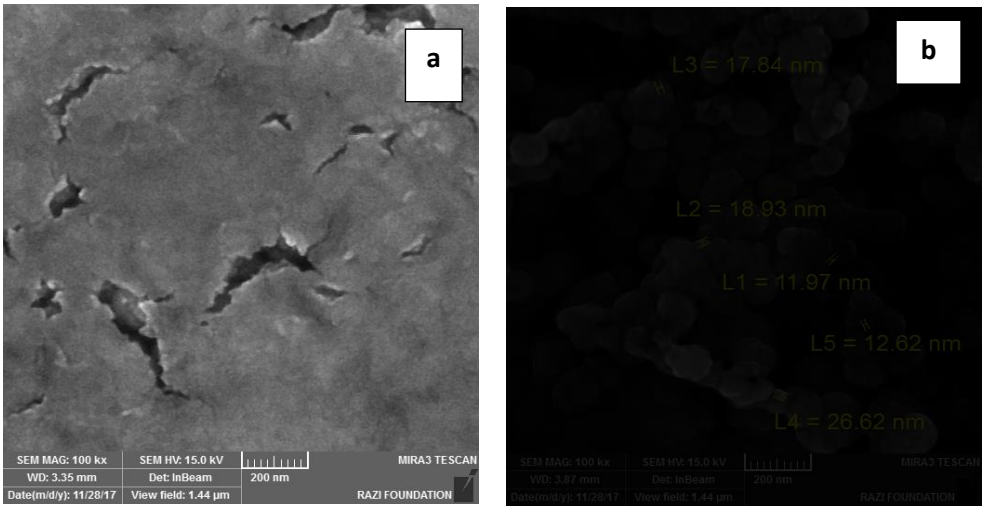

Figure 3: FESEM images of Co_3O_4:2wt. % Y_2O_3 thin film: (a) Seed layer, (b) Growth layer.

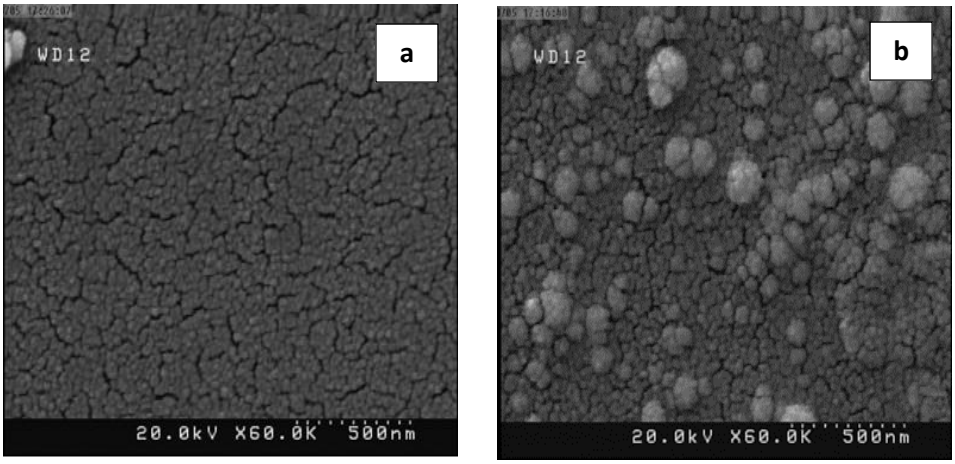

Figure 4: FESEM images of Co_3O_4:4wt.% Y_2O_3 thin film: (a) Seed layer, (b) Growth layer.

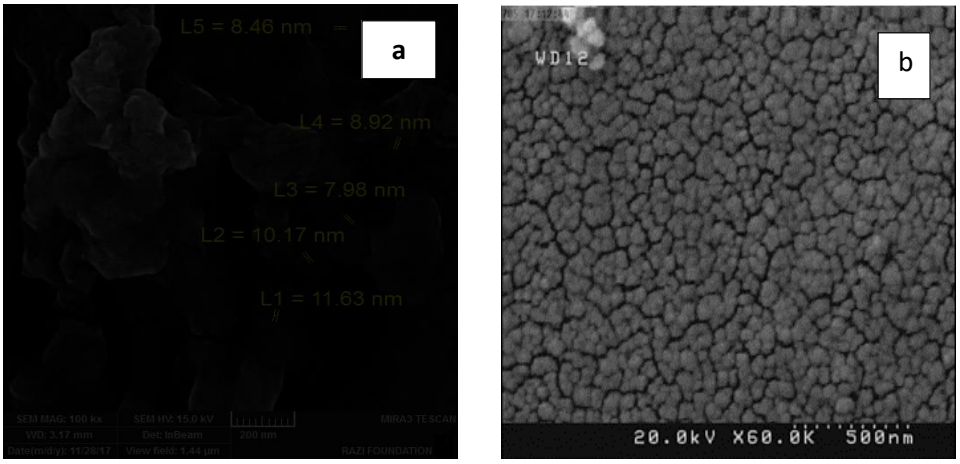

Figure 5: FESEM images of Co_3O_4:6wt. % Y_2O_3 thin film: (a) Seed layer (b) Growth layer.

3.3. Gas sensing measurement

The sensing properties of undoped Co_3O_4 nanoparticles and doped with (2, 4, and 6) % Y_2O_3 and deposited on n-type Si substrates were investigated, as a function of time and operating temperature, to find temperature dependence of sensitivity against oxidizing gas (NO_2) and reducing gas (H_2S). Hall measurements showed that undoped Co_3O_4 nanoparticles and doped with Y_2O_3 films were of a positive hall coefficient (p-type charge carrier). Fig.6 shows the variation of resistance as a function of time with on/off gas valve for sensors fabricated Co_3O_4:Y_2O_3 upon exposure to H_2S and NO_2 gases with concentration of 50 ppm at different operating temperatures starting from room temperature up to 250 ^oC with a gradual increase of 50 ^oC. The figures show a decrease in resistance values when the films were exposed to NO_2 gas, (Gas ON), then the resistance value increased at the closure of the gas (Gas OFF).

The reason for this behavior is the formation of oxygen ions as oxygen molecules on the surface of the metal oxides gain electrons from the metal oxides. The metal oxide surfaces have a hole accumulation layer for the p-type and electron depletion layer for the n-type. When oxidizing gases are introduced, the thickness of the electron-depletion layer increases. Thus, the resistance of n-type metal oxide gas sensor increased. Comparatively, the resistance of p-type metal oxide gas sensor decreased because of the increase in the hole accumulation layer. When reductive gases are introduced, the resistance of p-type metal oxide gas sensor increases because of the decrease in the hole accumulation layer [17, 18].

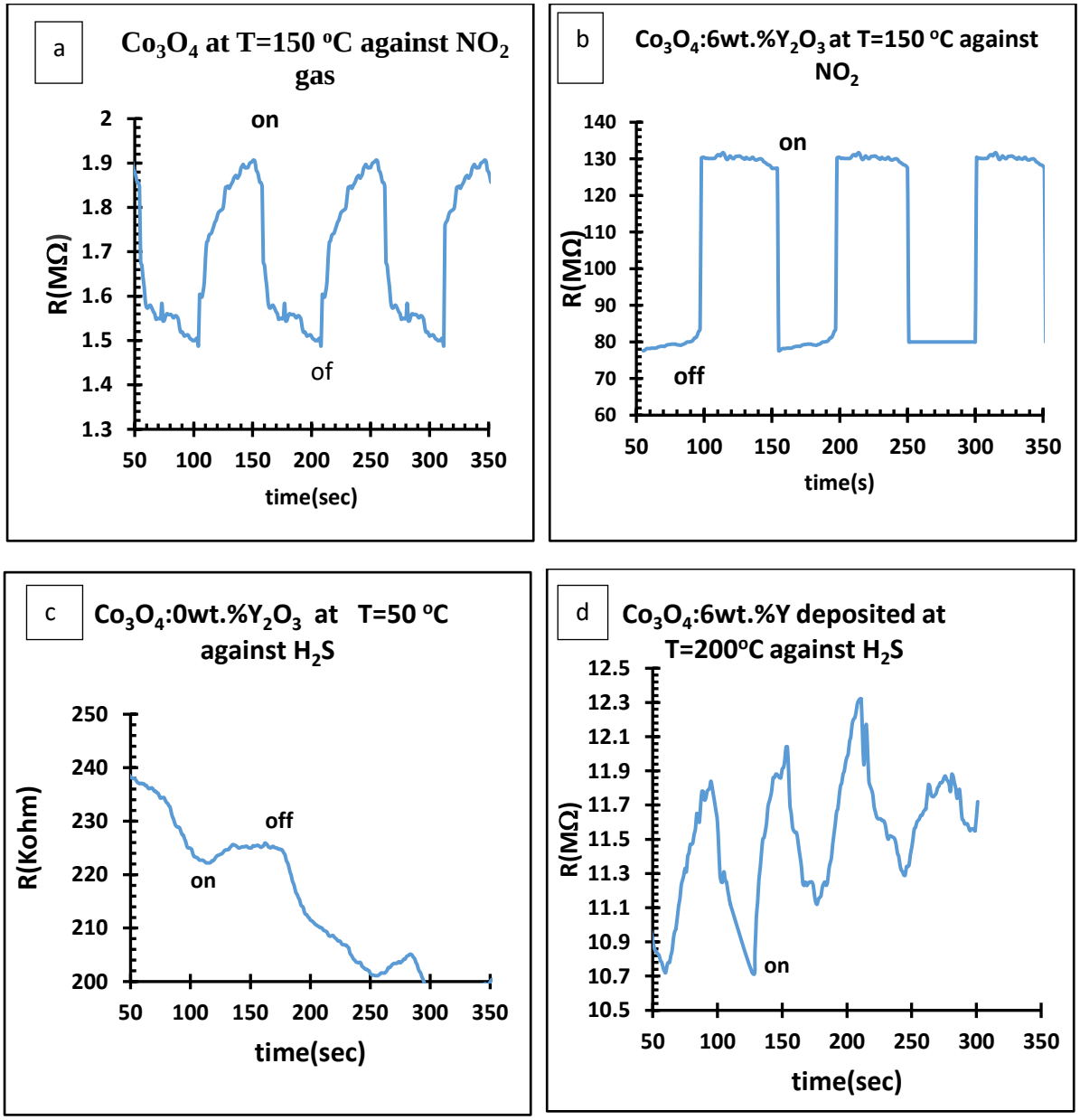

Figure 6: Variation of resistance with time for Co_3O_4:Y_2O_3 sensors upon exposure to NO_2 and H_2S gases at different operating temperature.

The sensitivity, response and recovery times depend on the operating temperature since temperature is responsible for the chemical kinetics in solid-gas reaction. The operating temperature is defined as the temperature at which the resistance of the sensor reaches a constant value. The changing of resistance is influenced only by the presence of some gases of interest. The sensitivity factor (S %) is calculated using the following equation [19]:

$$S = \left|\frac{R_g - R_a}{R_a}\right| * 100\% \qquad (4)$$

where S is the sensitivity, R_a and R_g are the electrical resistance of the film in air and the electrical resistance of the film in the presence of gas, respectively.

The response time of a gas sensor is defined as the time it takes the sensor to reach 90% of its maximum/minimum value of conductance upon the introduction of the

reducing/oxidizing gas. Similarly, the recovery time is defined as the time required to recover to within 10% of the original baseline when the flow of reducing gas is removed. The response time and recovery time can be calculated as follows [20]:

$$\boldsymbol{Respon\ time} = |\boldsymbol{t_{gas}(on)} - \boldsymbol{t_{gas}(off)}| \times \mathbf{0.9} \quad \textbf{(5)}$$

$$\boldsymbol{Recovery\ time} = |\boldsymbol{t_{gas}(off)} - \boldsymbol{t_{gas}(on)}| \times \mathbf{0.9} \quad \textbf{(6)}$$

Some sensors achieve fast response to input toxic gas which can be seen for square pulses instead of triangle pulses, also the repeatedity of the appearing pulses with time means excellent stability of these sensors against NO_2 and H_2S toxic gases. These results are listed in Tables 3 and 4. It is clear from theses tables that, the undoped Co_3O_4 and doped with different ratios of Y_2O_3 films, exhibited fast response speed of (0.8s) with recovery time of (0.8 s).

Table 3: Response time, recovery time and sensitivity of undoped Co_3O_4 and doped with (2, 4, and 6) % Y_2O_3 as a function of operating temperature upon exposure NO_2 gas.

Gas:NO_2 substrate: n-Si															
Y_2O_3 %	Sensitivity % at T_{op}					Response time (s) at T_{op}					Recovery time (s) at T_{op}				
	RT ^oC	50 ^oC	150 ^oC	200 ^oC	250 ^oC	RT ^oC	50 ^oC	150 ^oC	200 ^oC	250 ^oC	RT ^oC	50 ^oC	150 ^oC	200 ^oC	250 ^oC
0	0.57	5.5	1.9	1.5	6.3	24.3	0.8	11.7	16.2	0.8	14.4	0.8	8.1	26.1	0.8
2	0.95	7.5	7.9	7.7	5.8	22.2	28.8	15.3	0.8	34.2	13.2	20.7	28.8	0.8	36
4	5	5.4	42.7	15.1	7.31	0.8	38	24.3	9.9	54	0.8	36	21.6	24.3	37.8
6	3.09	17.0	62.5	6.5	28.5	13.5	0.8	0.8	18	0.8	9.9	0.8	0.8	34.2	0.8

Table 4: Response time, recovery time and sensitivity of undoped Co_3O_4 and doped with (2, 4, and 6) % Y_2O_3 as a function of operating temperature upon exposure H_2S.

Gas:H_2S substrate: n-Si															
Y_2O_3 %	Sensitivity % at					Response time (s) at					Recovery time (s) at				
	RT ^oC	50 ^oC	150 ^oC	200 ^oC	250 ^oC	RT ^oC	50 ^oC	150 ^oC	200 ^oC	250 ^oC	RT ^oC	50 ^oC	150 ^oC	200 ^oC	250 ^oC
0	0.62	2.6	2.15	2.21	10.58	0.8	22	29.8	10	5.4	0.8	18.15	25.71	25.61	32
2	37	22.1	25.9	23.2	21.07	16.2	9	0.8	0.8	0.8	18	18	0.8	0.8	0.8
4	4.07	9.5	3.7	4.2	4.1	37.6	26.4	31.7	---	41.8	54.4	49.2	41.8	--	36.9
6	90	3.28	7.7	9.3	8.62	0.8	27	35.6	27	0.8	0.8	25.2	50.2	21.6	0.8

The sensors results of this work, for NO_2 and H_2S gases. The Co_3O_4:6wt. %Y_2O_3 gives high sensitivity of (62.5%) at T=150^{o}C and fast response for NO_2 gas and gives high sensitivity of (90%) at RT and fast response for H_2S gas.

Doping can enhance gas sensitivity, as shown in most of the presented tables. Nonsystematic increase of gas sensitivity with yttria doping of cobalt oxide was detected. Because doping of metal oxides helps in improving their sensing characteristics by lowering the energy required for chemisorption of gas molecules on the semiconductor surface Adding an appropriate amount of yttria may increase the electron exchange rate. As mentioned, the crystallite size decreased with the increasing doping ratio which was confirmed by XRD measurement. Therefore, enhancement of sensitivity due to smallest crystallite and the reduction of crystallite

size might have influence on the width of space charge region that aids the chemisorption of gas molecules and sensing process. This result is in agreement with those of Yamazoe [17]. Operating temperature limits the sensing performance and characteristics of the thin film gas sensors. The operating temperature influences the receptor function through its effect on the chemical dynamics at gas-solid interface and thus determines the important sensing properties such as response, selectivity, stability, and response and recovery times [18].

4. Conclusions

Co_3O_4:Y_2O_3/n-Si nanostructure thin films sensor was synthesized using the hydrothermal method. The response of Co_3O_4:Y_2O_3/n-Si samples to hazardous H_2S and NO_2 toxic gases was studied.

Co_3O_4:6%Y_2O_3 has the smallest crystallite size and grain size. This sensor has good sensitivity to H_2S and NO_2 gases with a fast response time and recovery time. Its sensitivity to H_2S gas was 90 % at room temperature and 62.5% to NO_2 gas at 150 ^oC with 0.8 sec for both response and recovery times.

Acknowledgments

The authors wish to acknowledge the support rendered by the Laboratories of thin films in physical department, college of Science, Baghdad University.

Conflict of interest

Authors declare that they have no conflict of interest.

References

1. Neri G., *First fifty years of chemoresistive gas sensors.* Chemosensors, 2015. **3**(1): pp. 1-20.
2. Jiao M., *Microfabricated gas sensors based on hydrothermally grown 1-D ZnO nanostructures*, Thesis, Acta Universitatis Upsaliensis, 2017.
3. Wetchakun K., Samerjai T., Tamaekong N., Liewhiran C., Siriwong C., Kruefu V., Wisitsoraat A., Tuantranont A., and Phanichphant S., *Semiconducting metal oxides as sensors for environmentally hazardous gases.* Sensors and Actuators B: Chemical, 2011. **160**(1): pp. 580-591.
4. Kim H.-J. and Lee J.-H., *Highly sensitive and selective gas sensors using p-type oxide semiconductors: Overview.* Sensors and Actuators B: Chemical, 2014. **192**: pp. 607-627.
5. Vetter S., Haffer S., Wagner T., and Tiemann M., *Nanostructured Co3O4 as a CO gas sensor: temperature-dependent behavior.* Sensors and Actuators B: Chemical, 2015. **206**: pp. 133-138.
6. Jogade S., Sutrave D., and Patil V., *Structural and Morphological Properties of Mn-Doped Co3O4 Thin Film Deposited by Spin Coat Method.* IJERA, 2016. **6**(9): pp. 42-46.
7. Zhu X., Hou K., Chen C., Zhang W., Sun H., Zhang G., and Gao Z., *Structural-controlled synthesis of polyaniline nanoarchitectures using hydrothermal method.* High Performance Polymers, 2015. **27**(2): pp. 207-216.
8. Cosentino I. and Muccillo R., *Lattice parameters of thoria–yttria solid solutions.* Materials Letters, 2001. **48**(5): pp. 253-257.
9. Cheng C.-S., Serizawa M., Sakata H., and Hirayama T., *Electrical conductivity of Co3O4 films prepared by chemical vapour deposition.* Materials Chemistry and Physics, 1998. **53**(3): pp. 225-230.

10. Lakehal A., Bedhiaf B., Bouaza A., Benhebal H., Ammari A., and Dalache C., *Structural, optical and electrical properties of Ni-doped Co 3 O 4 prepared via Sol-Gel technique.* Materials Research (Sao Carlos, Online), 2018. **21**(3): pp. 1-8.
11. Hamdan S. and Ali I., *higher photo sensitivity of co-y-oxide nano structure synthesized by hydrothermal method.* Digest Journal of Nanomaterials & Biostructures (DJNB), 2018. **13**(3).
12. Jaffer Sadiq M.M. and Samson Nesaraj A., *Reflux condensation synthesis and characterization of Co3O4 nanoparticles for photocatalytic applications.* Iranian Journal of Catalysis, 2014. **4**(4): pp. 219-226.
13. Yarestani M., Khalaji A., Rohani A., and Das D., *Hydrothermal synthesis of cobalt oxide nanoparticles: Its optical and magnetic properties.* Journal of Sciences, Islamic Republic of Iran, 2014. **25**(4): pp. 339-343.
14. Farhadi S., Javanmard M., and Nadri G., *Characterization of cobalt oxide nanoparticles prepared by the thermal decomposition.* Acta Chimica Slovenica, 2016. **63**(2): pp. 335-343.
15. Shinde V., Mahadik S., Gujar T., and Lokhande C., *Supercapacitive cobalt oxide (Co3O4) thin films by spray pyrolysis.* Applied Surface Science, 2006. **252**(20): pp. 7487-7492.
16. Gujar T., Shinde V., Lokhande C., Mane R., and Han S.-H., *Bismuth oxide thin films prepared by chemical bath deposition (CBD) method: annealing effect.* Applied surface science, 2005. **250**(1-4): pp. 161-167.
17. Yamazoe N., *New approaches for improving semiconductor gas sensors.* Sensors and Actuators B: Chemical, 1991. **5**(1-4): pp. 7-19.
18. Kannan S., Rieth L., and Solzbacher F., *NOx sensitivity of In2O3 thin film layers with and without promoter layers at high temperatures.* Sensors and Actuators B: Chemical, 2010. **149**(1): pp. 8-19.
19. Patil L.A., Bari A.R., Shinde M.D., Deo V.V., and Amalnerkar D.P., *Synthesis of ZnO nanocrystalline powder from ultrasonic atomization technique, characterization, and its application in gas sensing.* IEEE Sensors journal, 2010. **11**(4): pp. 939-946.
20. Patil D., Patil L., Jain G., Wagh M., and Patil S., *Surface activated ZnO thick film resistors for LPG gas sensing.* Sensors & Transducers, 2006. **74**(12): pp. 874-883.

استجابة الغازات السامة للأغشية الرقيقة ذات البنية النانوية لأكسيد الكوبالت

سهاد عبد الكريم حمدان، افتخار محمود علي، عصام محمد ابراهيم
قسم الفيزياء، كلية العلوم، جامعة بغداد، بغداد، العراق

الخلاصة

تم فحص خصائص الاغشية النانويةCo_3O_4 غير المطعمة و المطعمة بY_2O_3لاستشعار الغازات. صنعت الأغشية باستخدام طريقة الهيدروثرمل على طبقة البذرة. فحصت خصائص تحليل XRD و SEM واستشعار الأغشية الرقيقة المحضرة للغاز.اوضح فحص XRD أن جميع الاغشيةمتعددة البلورات بطبيعتها، ولها هيكل مكعب، وأن الحجم البلوري (12.6) نانومتر لأكسيد الكوبالت و (12.3) نانومتر للنسبة لاوكسيد الكوبلت المطعم ب Y_2O_3٪6. من الواضح أن تحليل SEM للأغشية الرقيقة يشير إلى أن جميع الاغشية المطعمة والغير مطعمة تمتلك بنية كروية الشكل.

تم اختبار الحساسية ووقت الاستجابة ووقت الاسترداد للغازات H_2S و NO_2 عند درجات حرارة تشغيل مختلفة. تتغير المقاومة مع التعرض لغاز الاختبار. أظهرت النتائج أن Co_3O_4: ٪ 6Y_2O_3 يمتلك أعلى حساسية حوالي 90٪ عند درجة حرارة الغرفة و 62.5٪ عند 150 درجة مئوية عند التعرض للغاز المختزلH_2S والغاز المؤكسد NO_2 على التوالي مع 0.8 ثانية لكل من أوقات الاسترداد والاستجابة.